Journal of Hydroscience and Hydraulic Engineering
Vol. 16, No. 1, May, 1998, 27-39

IMPACTS OF MICROCLIMATE MODIFICATION OVER AN IRRIGATED LAND IN ARID AREA DURING SUMMER

By

Takeshi Fujino

Research Associate, Graduate School of Science and Engineering,
Saitama University, Urawa, Saitama, 338, Japan

Takashi Asaeda

Associate Professor, Graduate School of Science and Engineering,
Saitama University, Urawa, Saitama, 338, Japan

and

Akio Wake

Chief Research Engineer, Environmental Engineering Division,
Shimizu Corporation, Koto-ku, Tokyo, 135, Japan

SYNOPSIS

Meteorological field observations were conducted at an irrigated alfalfa farm in arid area to evaluate the possible mitigation of summer heat by the greenery. Atmosphere over the farm found to be always under stable conditions because the surface temperature was always lower than air temperature. Air temperature decreased *5 degrees* from the upwind edge of the farm to its downwind edge of the farm. The heat balance of the region was analyzed in detail and a three-dimensional meso-scale atmospheric model was developed for numerical simulation of the micro-meteorological change that was found by would the measurement. Evapotranspiration from the farm was estimated to be more than *10 mm/day*.

INTRODUCTION

Irrigation using recycled or reused water resources has already been practiced in some desert regions around the world, contributing to production of crops in otherwise infertile lands. This type of irrigation in arid lands is beginning to attract attention in anticipation of severe world food shortages associated with rapid population growth. From a micro-climatic perspective, on the other hand, it is possible to envision that large-scale irrigation of natural desert regions could provide some moderation of summer heat by favorably modifying the thermal properties of the ground (Wake, 1995). The objective of the present study is to investigate quantitatively the possible mitigation of summer heat in desert land. This study presents a partial result of the field observation undertaken during the summer of 1995, at the Sulaibiya Farm near Kuwait City. The analysis for this study utilizes a one-dimensional heat balance model, and three-dimensional meso-scale atmospheric model.

METEOROLOGICAL OBSERVATION AT SULAIBIYA FARM

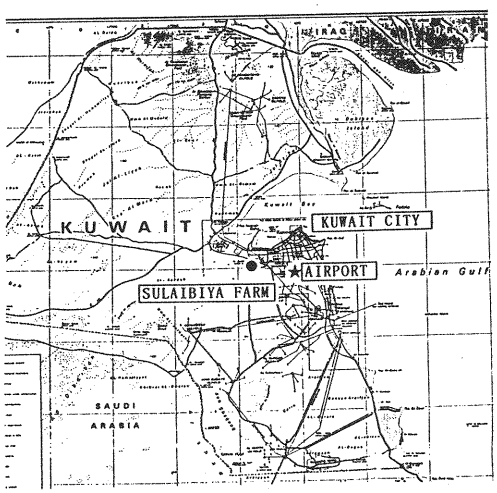

Fig. 1 Location of observation site

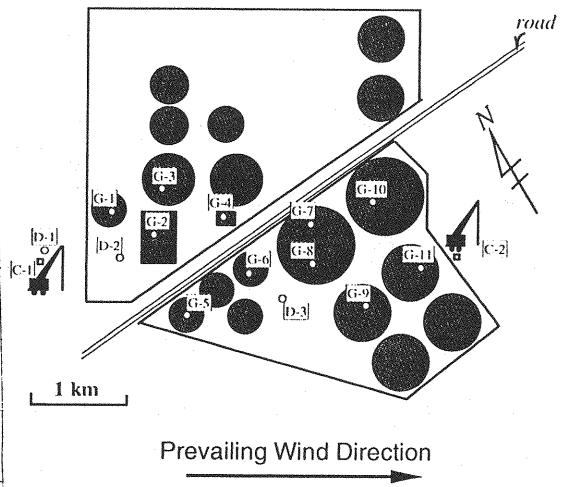

D:Desert G:Alfalfa C:Crane

Fig. 2 Measurement sites at Sulaibiya farm

Locations of Observation Sites

Sulaibiya Farm(*29. 15 N, 47. 45 E*) is located approximately *25 km* West of Kuwait City (Fig. 1) and consists of 18 circular and two rectangulars alfalfa fields spreading over *6 km* in the Sulaibiya area (Fig. 2). The radii of the circular farms range from *220 m* to *490 m*, and the area of the rectangular field is about *250, 000 m²*. Each of the alfalfa fields is irrigated by secondary-treated municipal waste water sprinkled by large-scale pivoted arms at an average rate of *12 mm/day*. In average, the crop is harvested every *21-day* when the height of the grass reaches about *30 cm*. The locations of observation sites are indicated by white dots in Fig. 2. Three unirrigated barren sites, marked with 'D' in the figure, were also included as controls. The one of the control sites, 'D-1', is located in a desert ground northwest of the Farm in the upwind of the prevailing wind. In addition, vertical temperature profiles up to *50 m* were measured at two locations upwind (C-1) and downwind (C-2) of the Farm.

Observation Method

Field observations in Sulaibiya were conducted over 11 days: Aug. 28, to Sept. 4, and Sept. 8 to 10, 1995. At the sites marked by 'D' and 'G' in Fig. 2, the measurements were conducted for solar radiation; ground albedo; net radiation; air temperature, relative humidity, wind vector at a height of the order of 1m; surface and soil temperature, and soil water content. The instruments and devices used are: albedo meters (MR-22, EKO); net radiation meters (CN-11, EKO); thermo-recorders (TH-10, TABAI ESPEC) for air temperature and humidity; anemometers (Makino), and thermo couples (CHINO) for soil temperature. The measurements were automatically recorded by data loggers except for the soil water content.

Table 1 shows the observation periods, heights, and recording intervals. For the air temperature measurements, thermo-recorders were installed at 11 locations over alfalfa fields (G-1 through G-11), and 3 locations at unirrigated control sites (D-1 through D-3). The soil temperature profiles were measured by placing thermocouple trees at two locations, one inside the alfalfa field (G-9) and the other in the desert (D-1). On September 3 and 4, vertical air temperature profiles up to *50 m* were continuously measured for 24 hours at the two control sites, up-and downwind of the farm (C-1 and C-2).

Table 1 Instrumentation of the field observation at Sulaibiya in 1995

Desert

Observation Items	Period	Level	Record Interval
Dry and Wet Temperature	Aug.28~Sept.4	above 1.5 m	1 min.
Wind Speed and Direction	Aug.28~Sept.4	above 1.5 m	1 min.
Solar Radiation	Aug.30~Sept.4	above 1.5 m	1 min.
Surface Albedo	Aug.30~Sept.4	above 1.5 m	1 min.
Net Radiation	Aug.30~Sept.4	above 0.3 m	1 min.
Soil Temperature	Aug.29~Sept.4	below 1,5,10,20,30,40 cm	1 min.
Vertical Temperature	Sept.3~Sept.4	above 10,20,30,40,50 m	30 sec.

Alfalfa Field

Observation Items	Period	Level	Record Interval
Dry Temperature	Aug.28~Sept.4	above 1.5 m	1 min.
	Sept.8~Sept.10		
Wet Temperature	Aug.28~Sept.4	above 1.5 m	1 min.
	Sept.8~Sept.10		
Wind Speed and Direction	Aug.28~Sept.4	above 1.5 m	1 min.
Solar Radiation	Aug.28~Aug.30	above 1.5 m	1 min.
Sueface Albedo	Aug.28~Aug.30	above 1.5 m	1 min.
Net Radiation	Aug.28~Aug.30	above 0.3 m	1 min.
Soil Temperature	Aug.29~Sept.4	below 1,5,10,20,30,40 cm	1 min.
	Sept.8~Sept.10	below 1cm	1 min.
Vertical Temperature	Sept.3~Sept.4	above 10,20,30,40,50 m	30 sec.
Water Content	Aug.30~Sept.3	below 5,20 cm	once a day

RESULTS

Radiation Balance

Throughout the observation period, the sky remained clear. Figure 3 shows the net radiation at the alfalfa field and at the desert site. The solar radiation reached a maximum of *950W/m²* between noon and 1 p.m.. The surface albedo was approximately 0.30 for the desert and 0.15 for the alfalfa field, and it was found to be insensitive to the solar angle except at dawn and twilight. The net absorption of radiation (short- and longwave) was greater for the alfalfa field than for the desert surface throughout the day. The maximum net absorbed radiation was *440W/m²* in the desert and *650W/m²* in the alfalfa field.

Wind Direction and Speed

The prevailing wind direction was between *WNW* and *NNW* throughout the observation period, as commonly is the case during the summer in the area. The daily average wind speed varied little between *3.0 m/s* and *4.0 m/s* during the period, and the daily maximum averaged about *6.0m/s*, and peaked to *10 m/s* at one occasion. The wind generally turned stronger during the night. Figure 4 shows the recorded wind speeds on Sept. 3. The wind speed record at the Airport, about *20 km* east of the site, is also shown as a reference.

Soil Temperature

Figures 5 and 6 show the soil temperature profiles at the desert and the alfalfa field sites. The soil temperature at *1cm* below the ground in the desert reached a maximum of *54 °C* during the day, and dropped to a minimum of *26 °C* before the dawn. The amplitude

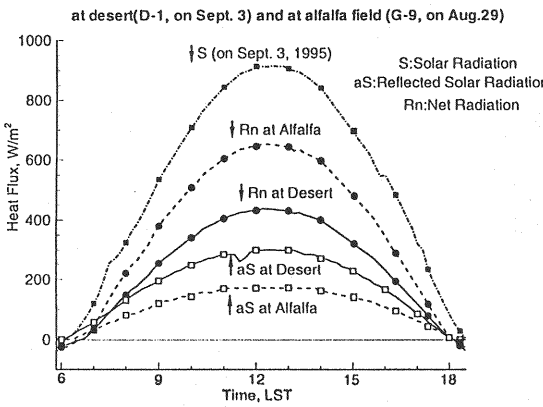

Fig. 3 Radiation Balance

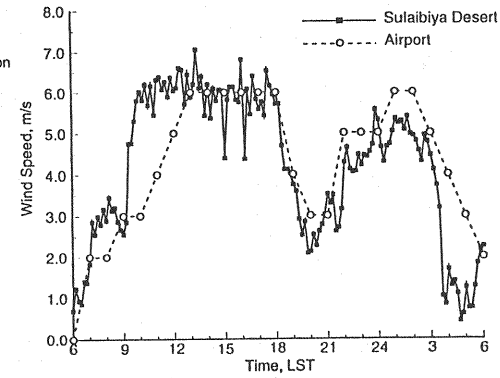

Fig. 4 Wind Speed on Sept. 3, 1995

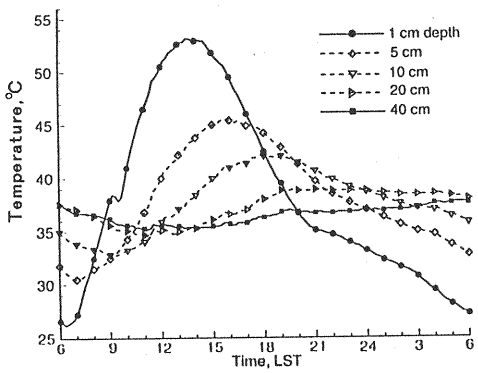

Fig. 5 Ground Temperature at Desert on Sept. 3, 1995

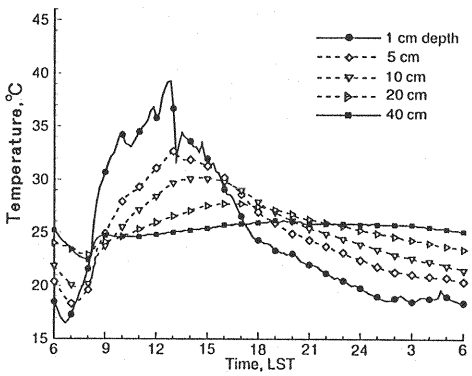

Fig. 6 Ground Temperature at Alfalfa Field on Sept. 3, 1995

of daily temperature change diminished with soil depth. At a depth of *40 cm*, ground temperature stayed nearly constant at about *37 °C*. The surface temperature at the alfalfa field peaked at less than *40 °C* during the day, and dropped to less than *20 °C* before the dawn. In **Figure 6**, the sudden spike-like drops in the surface temperature resulted from the sprinkler sprays. At a depth of *40cm* in the alfalfa field was also almost steady at about *25 °C*, which is lower than the desert site in more than *10 °C*. **Figure 7** shows the soil surface temperature underneath the alfalfa growth on Sept. 9. The maximum ground surface temperature, in this case, was about *30 °C*, about *7 °C* lower than the case when the alfalfa growth was removed.

Air Temperature

Figures 8 and **9** show the air temperature and relative humidity near the ground at the desert, and the farm sites as well as at the Airport. The wind, the temperature, and the humidity variations at the desert site closely correspond to those at the Airport. The desert site appears to be representative of the inland climate of the area. The low-level air temperatures at the alfalfa sites were decidedly lower than at the desert site. It can be found in the figure that the air temperature decreases with distance in the downwind direction. The maximum for the day was about *44 °C* at the desert and less

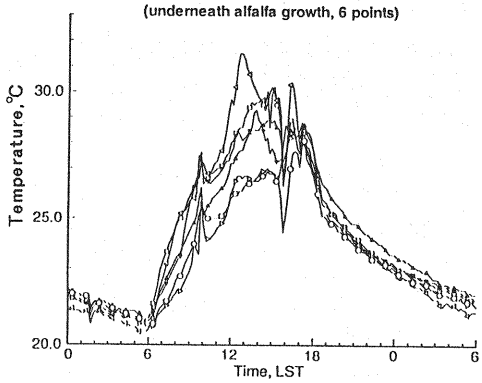

Fig. 7 Ground Temperature at Alfalfa Field on Sept. 9, 1995

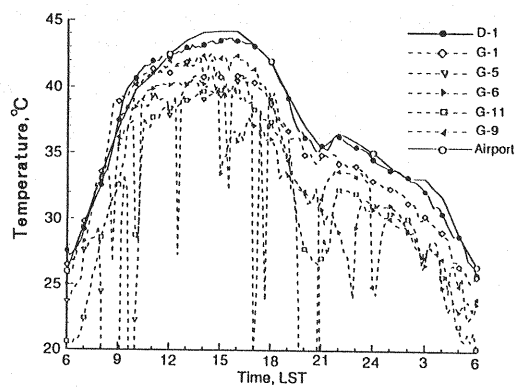

Fig. 8 Air Temperature on Sept. 3, 1995

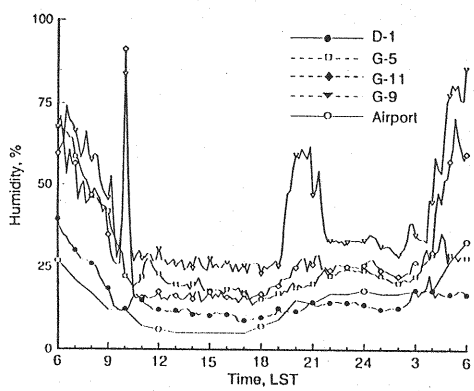

Fig. 9 Relative Humidity on Sept. 3, 1995

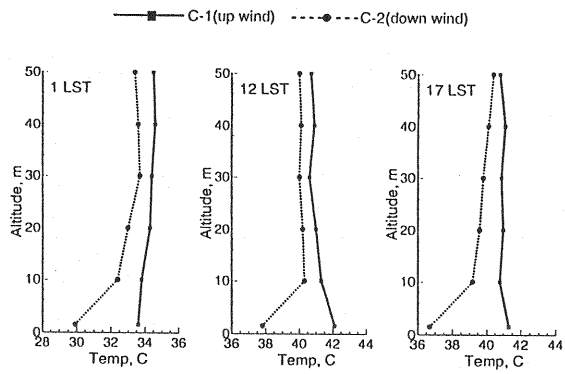

Fig. 10 Vertical Air Temperature on Sept. 4, 1995

at the downwind edge of the farm. Relative humidity distributions show a tendency to increase, inversely with the distance from the upwind edge of the farm.

Vertical Air Temperature Profiles

Figure 10 shows the vertical air temperature profiles measured with thermo-recorders hanged from *50 m* cranes at the up- and downwind sites of the Farm (C-1 and C-2 in Fig. 2). At the downwind site, it is found that ground surface temperature was lower than the low-level air temperature, indicating that the ground-level atmosphere remained stable throughout the 24-hour period. Although the air temperatures at the downwind site were persistently lower than those at the upwind site, the significant differences were confined to the lower *10 m* above the ground.

HEAT BALANCE ANALYSES

Thermal Properties of Soil

The thermal properties of the ground in the area were evaluated numerically by the heat balance method at the air/ground interface. The net radiative energy at the interface

Table 2 Soil characteristics

Item	Heat Capasity ($J/cm^3/K$)	Heat Conductivity ($W/m/K$)	Water Content (g/g)
Dry sand(Desert)	2.88	0.36	0.0
Wet sand(Alfalfa Field)	4.60	2.40	0.18

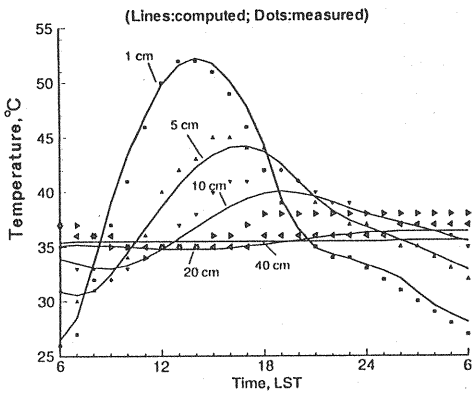

Fig. 11 Ground Temperature at Desert for Sept. 3, 1995

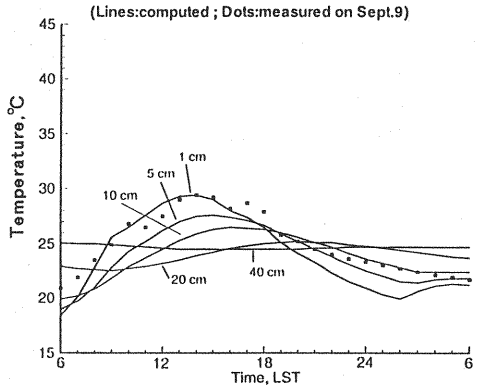

Fig. 12 Ground Temperature at Alfalfa for Sept. 3, 1995

was divided into sensible, latent, and ground heat fluxes. The sensible and latent heat fluxes were calculated by Louis (1979)'s analytical method, and the soil heat flux was evaluated directly from the heat balance. The soil temperature profile down to the depth of *50 cm* was evaluated by solving the one-dimensional heat conduction equation with *1 cm* mesh. As the lower boundary condition, the temperature at the lowest mesh was set as a constant value, which is confirmed by the field measurements as described in the earlier section. The thermal conductivity and the heat capacity of the soil at the desert site were evaluated by calibrating the set of equations using the measured data. Table 2 shows the results. The calculated thermal conductivity matches the general value for desert sand found in literature(e.g. Eagleson, 1970), while the calculated heat capacity was slightly greater than the general value.

Analyses of Soil Temperature Profiles

Figures 11 and 12 are the simulated results of the ground temperature profiles at the desert and the alfalfa sites for Sept. 3, respectively. At the desert site, as the water content of the soil can be considered nearly zero, its thermal properties were assumed homogeneous. The upper boundary condition was derived from the heat budget at the surface. The calculated results reproduced the measured profiles well. At the alfalfa field site, a Dirichlet-type upper boundary condition was used the basis of the measured temperature. For the alfalfa site, thermal conductivity and heat capacity of the soil were evaluated from the measured values of soil water content. For both the desert and the alfalfa sites, the simulations reproduced the measured results well. The variation of soil temperature is considerably smaller both in terms of time and space at the alfalfa site than at the desert site, as expected from the larger soil water content.

Heat Balance

Figures 13 and 14 show the heat balance variation at the desert and the alfalfa sites

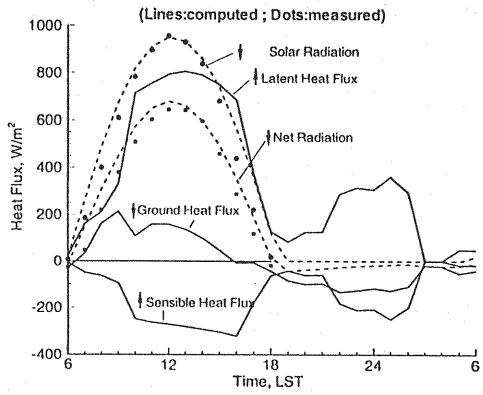

Fig. 13 Heat Balance at Desert for Sept. 3, 1995

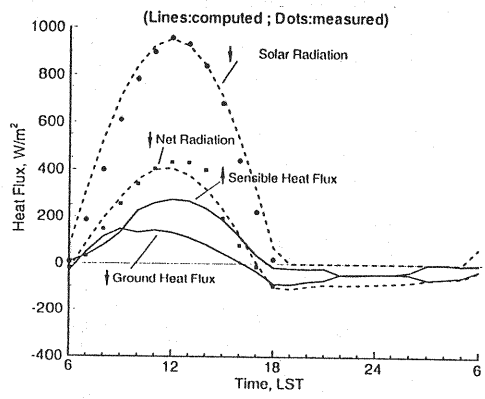

Fig. 14 Heat Balance at Alfalfa for Sept. 3, 1995

evaluated from the measured data. At the desert site, without the presence of latent heat transfer, the net radiative energy is decomposed into only two components: sensible heat and ground heat fluxes. The maximum rate of the sensible heat flux reached about *300 W/m²* during the daytime. Around midnight, from 22 LST to 2 LST, the ground surface absorbed the sensible heat from the air at a rate of *60 W/m²*, as the surface temperature became lower than that of the air and the strong winds enhanced the turbulence. As a result, the net radiation stayed almost const and the ground heat flux increased during this period. At an alfalfa field, on the other hand, the latent heat flux is greater than the net radiation energy, reaching a maximum rate of about *900 W/m²*. The sensible heat flux was found to be always negative, meaning that heat was supplied from the air to the ground at a maximum rate of about *350 W/m²*. In the night, the latent heat flux was released from the ground when the wind was strong. Consequently, the sensible heat transfer to the ground increased during this period. This is, again, due to enhanced turbulence with strong wind. The daily total evapotranspiration was about *11.5 mm*, indicating that nearly *95 %* of the supplied water evaporated. At a alfalfa field in Arizona during a peak summer, Van Bavel (1966) estimated the maximum latent heat flux at around *800 W/m²*, and the total evapotranspiration at about *12 mm/day* under windy conditions, and at about *8.5 mm/day* under calm conditions. Norman, et al. (1978) also studied the water balance of an alfalfa field in Nebraska during a summer and estimated that the maximum latent heat flux was about *900 W/m²* with *11 mm/day* of total evapo-transpiration. The results of the present analyses for Sulaibiya Farm are comparable to these data.

AIR TEMPERATURE AND WIND FIELDS ANALYSES

The Governing Equations

The numerical model employed in the present study is referred to as a 'second-moment turbulence closure model' based on Mellor and Yamada(1974). The model parameters are wind, potential temperatures, mixing-ratio of water vapor, second moments of turbulence, and turbulent transport coefficients. Assumptions employed in the model are: (1) hydrostatic equilibrium, and (2) the Boussinesq approximation.

The governing equations, in the terrain-following vertical transformed coordinate system are given by

$$\frac{DU}{Dt} = f(V - V_g) + g\frac{\overline{H} - z^*}{\overline{H}}\left(1 - \frac{\langle\Theta_v\rangle}{\Theta_v}\right)\frac{\partial z_g}{\partial x} + \frac{\partial}{\partial x}\left(K_x\frac{\partial U}{\partial x}\right) + \frac{\partial}{\partial y}\left(K_{xy}\frac{\partial U}{\partial y}\right) + \frac{\overline{H}}{\overline{H} - z_g}\frac{\partial}{\partial z^*}(-\overline{uw}), \quad (1)$$

$$\frac{DV}{Dt}=-f(U-U_g)+g\frac{\overline{H}-z^*}{\overline{H}}\left(1-\frac{\langle\Theta_v\rangle}{\Theta_v}\right)\frac{\partial z_g}{\partial x}+\frac{\partial}{\partial x}\left(K_{xy}\frac{\partial V}{\partial x}\right)+\frac{\partial}{\partial y}\left(K_x\frac{\partial V}{\partial y}\right)+\frac{\overline{H}}{\overline{H}-z_g}\frac{\partial}{\partial z^*}(-\overline{vw}), \quad (2)$$

$$\frac{\partial U}{\partial x}+\frac{\partial V}{\partial y}+\frac{\partial W^*}{\partial z^*}-\frac{1}{\overline{H}-z_g}\left(U\frac{\partial z_g}{\partial x}+V\frac{\partial z_g}{\partial y}\right)=0, W^*\equiv\frac{\overline{H}}{\overline{H}-z_g}W+\frac{z^*-\overline{H}}{\overline{H}-z_g}\left(U\frac{\partial z_g}{\partial x}+V\frac{\partial z_g}{\partial y}\right), \quad (3)$$

$$\frac{D\Delta\Theta}{Dt}=\frac{\partial}{\partial x}\left(K_x\frac{\partial\Delta\Theta}{\partial x}\right)+\frac{\partial}{\partial y}\left(K_y\frac{\partial\Delta\Theta}{\partial y}\right)+\frac{\overline{H}}{\overline{H}-z_g}\left[\frac{\partial}{\partial z^*}(-\overline{w\theta})+\frac{1}{\rho C_p}\frac{\partial R_N}{\partial z^*}-W\frac{\partial\Theta_v}{\partial z}\right], \quad (4)$$

$$\frac{DQ_v}{Dt}=\frac{\partial}{\partial x}\left(K_x\frac{\partial Q_v}{\partial x}\right)+\frac{\partial}{\partial y}\left(K_y\frac{\partial Q_v}{\partial y}\right)+\frac{\overline{H}}{\overline{H}-z_g}\frac{\partial}{\partial z^*}(-\overline{wq_v}), \quad (5)$$

$$\frac{D}{Dt}\left(\frac{e^2}{2}\right)=\frac{\partial}{\partial x}\left[K_x\frac{\partial}{\partial x}\left(\frac{e^2}{2}\right)\right]+\frac{\partial}{\partial y}\left[K_y\frac{\partial}{\partial y}\left(\frac{e^2}{2}\right)\right]+\left(\frac{\overline{H}}{\overline{H}-z_g}\right)^2\frac{\partial}{\partial z^*}\left[elS_q\frac{\partial}{\partial z^*}\left(\frac{e^2}{2}\right)\right]$$
$$-\frac{\overline{H}}{\overline{H}-z_g}\left(\overline{uw}\frac{\partial U}{\partial z^*}+\overline{vw}\frac{\partial V}{\partial z^*}\right)+\beta g\overline{w\theta_v}-\frac{e^3}{B_1 l}, \quad (6)$$

$$-\overline{uw}=le\tilde{S}_M\frac{\partial U}{\partial z} \quad (7)$$

$$-\overline{vw}=le\tilde{S}_M\frac{\partial V}{\partial z} \quad (8)$$

$$-\overline{w\theta}=\alpha le\tilde{S}_M\frac{\partial\Theta}{\partial z} \quad (9)$$

$$-\overline{wq_v}=\alpha le\tilde{S}_M\frac{\partial Q_v}{\partial z} \quad (10)$$

where U, V, W: wind components for x, y, z direction; Θ_v: virtual potential temperature; Q_v: mixing ratio of water vapor; u, v, w, θ_v, q_v: deviation components of U, V, W, Θ_v, Q_v; e^2: twice of turbulent kinetic energy; $-uw$, $-vw$, $-w\theta_v$, $-wq_v$; f: Corioli's parameter; U_g, V_g: geostrophic wind components; K_x, K_{xy}, K_{yy}: horizontal eddy viscosity; g: acceleration of gravity; β: the thermal expansion coefficient; ρ: the air density; ρC_p: the heat capacity of air; R_N: net radiation; W^*: vertical component of winds in the transformed coordinate; z^*: transformed vertical coordinate; z_g: ground elevation; H: material surface of the model in z^*-coordinate; l: turbulent length; α: turbulent plandtl number; S_M: stability function; B_1, S_q: empirical constants; $\langle\rangle$ indicates an average over a horizontal surface.

The ground surface boundary conditions are obtained from the empirical formulae by Dyer and Hicks(1970) for the nondimensional wind, air temperature, and mixing ratio profiles based on the similarity theory. Implementation of the similarity formulae into the model requires knowledge of ground surface temperatures. The temperature distribution within the soil layer is determined by solving the usual heat conduction equation and the heat balance equation:

$$\rho_s C_s\frac{\partial T}{\partial t}=K\frac{\partial^2 T}{\partial z^2}, \quad (11)$$

$$-K\frac{\partial T}{\partial z}=S(1-\alpha)+R_{Ln}+H+L_eE, \quad (12)$$

where, z is positive downward; T: soil temperature; $\rho_s C_s$: the heat capacity of soil; K: the heat conductivity of soil; S: solar radiation; a: surface albedo; R_{Ln}: net long-wave radiation; H: sensible heat flux; L_eE: latent heat flux. The lower boundary condition in Eq. (11) is a constant temperature at a sufficient depth obtained by measurement. Sensible heat flux and latent heat flux are given by

$$H=-\rho C_p u_* t_*, \quad (13)$$

$$L_eE = -\rho L_e u_* q_*, \tag{14}$$

where u_*, t_* and q_* are the friction velocity, temperature and water vapor scale, respectively, and are based on the similarity theory (Garratt and Hicks, 1973) given by

$$u_* = \kappa \left(U_{z_1}^2 + V_{z_1}^2\right)^{1/2} \left[ln\frac{z_1}{z_0} - \Psi_m\right]^{-1}, \tag{15}$$

$$t_* = \frac{\kappa}{P_r} (\Theta_{z_1} - \Theta_G) \left[ln\frac{z_1}{z_{0t}} - \Psi_h\right]^{-1}, \tag{16}$$

$$q_* = \frac{\kappa}{P_r} (Q_{z_1} - Q_G) \left[ln\frac{z_1}{z_{0t}} - \Psi_h\right]^{-1}. \tag{17}$$

in which z_1 and G are the reference height and the surface, respectively. P_r : the turbulent Prandtl number under neutral stability; κ : von Karman constant; z_0, z_{0t}: the roughness length for momentum and heat and/or moisture; Ψ_m, Ψ_h : the integrated stability correction terms for momentum and heat and/or moisture (Panofsky, 1963). The remainder of mixing ratio between surface and z_1 is rewritten by the so-called β-method (Kondo et al., 1990),

$$Q_{z_1} - Q_G = \beta_e (Q_{z_1} - Q_{Gsat}), \tag{18}$$

where β_e is the coefficients representing the surface moisture availability, and Q_{Gsat} is the saturated specific humidity at the soil surface temperature.

Numerical Method and Initial Conditions

The governing equations along with the boundary and initial conditions are discretized in time and space using the second-order finite difference and are solved by ADI (Alternating direction implicit) technique. The soil temperature distribution is computed by one-dimensional finite volume method with implicit time-integration. The *27.6km×19.6km* computational domain is discretized horizontally by a nested grid system consisting of overlapped primary (*400m×400m*), secondary (*100m×100m*) mesh resolutions. This nesting method enables finer resolution in area of interest while covering an area large enough to account for the secondary mesh of boundary effects. The vertical domain was discretized to an altitude of *4000m* using a variable mesh spacing composed of *26* nodes. For soil temperature computation, variable spacing was also applied with *14* nodes extending to a depth of *1.2m*.

An initial vertical wind profile at a reference site within the computational domain is first constructed by assuming a logarithmic profile (initially with u_*=*0.2m/s*, and z_0=*0.01m*) from the ground up to the level where the wind speed reaches an ambient value (geostrophic wind). Wind profiles at other grid positions are obtained by calibrating the profile at the reference site to satisfy the mass continuity. The vertical profile of potential temperature is initially assumed to increase linearly with height and to be uniform in the horizontal directions. Initial value for water vapor is distributed by using the initial potential temperature profiles, pressure at a reference site, and observed relative humidity. The kinetic energy and length scale are initialized by using the wind and temperature profiles according to the procedure of *level 2.5 model* (Yamada, 1983). The effects of imprecision in the initial conditions diminish rapidly within a few hours of time integration and self-corrected. For the value of other physical parameters, e.g. surface albedo, short-and long-wave radiation, and soil parameters, the measured or estimated value was used.

Computation Results

Figure 15 shows the computed horizontal surface temperature distributions at *15:00*

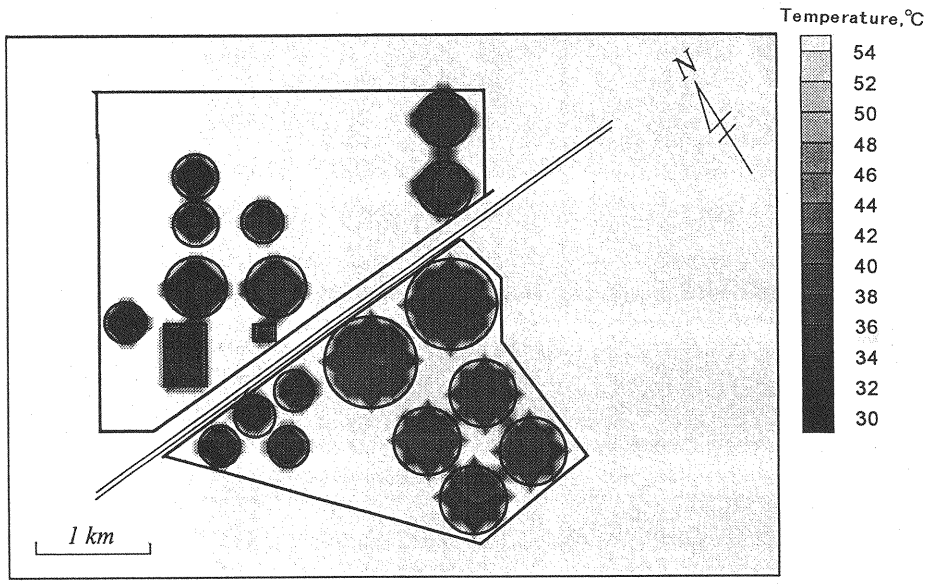

Fig. 15 Computed Surface Temperature at 15:00 for Sept. 3.

LST. The obvious contrast of the air temperature between the desert and the alfalfa field are clearly reproduced. The distributions of each surface are almost homogeneous because the thermal properties of each ground are assumed to be same, even air temperature and wind vectors at a reference level will be different from the place to place. Figure 16 is computed horizontal distributions of temperature and wind vectors at a selected time level. The temperature contours represent values at *1.5m* above the surface while the wind vectors indicate magnitudes and directions at *6.0m* height. The air temperature of the area reaches the maximum at this time as predicted by the heat balance analyses (Fig. 11). The low-level air temperatures are significantly different upwind and downwind of the farm, even the greenery is divided in places. Weak but effective downward convection is generated in the farm area. This, in turn, produces ground-level outflow of cooled air from the site. The drastic air temperature reduction, even in the exterior of the site can be explained by the evapotranspiration effect. Figure 17 shows the computed air temperature and wind structures at the same time in the vertical plain up to *50m* height along the cross-section of the center of the farm. Formations of several cool islands can be clearly observed over the each alfalfa field. The thermal boundary layer is gradually developed along the wind direction. The strong temperature differences between the surface and *10m* height, rapidly decrease over the height as well as the observation results shown in Fig. 10.

CONCLUSION

A field observation of micro-meteorological mitigation by greenery was conducted at Sulaibiya Farm. The ground surface temperatures of the alfalfa fields were lower than the air temperature throughout the observation period, indicating that the low-level atmosphere in the area was consistently stable even in the daytime. In addition, the development of thermal boundary layer was observed by the trend that the daytime ground level air temperature was lower with the downwind distance in the farm. A maximum of *5 °C* difference was recorded between the up- and the downwind of the farm over a fetch of *3 km*. The mitigation effects of the alfalfa field on the upper air was also recognized.

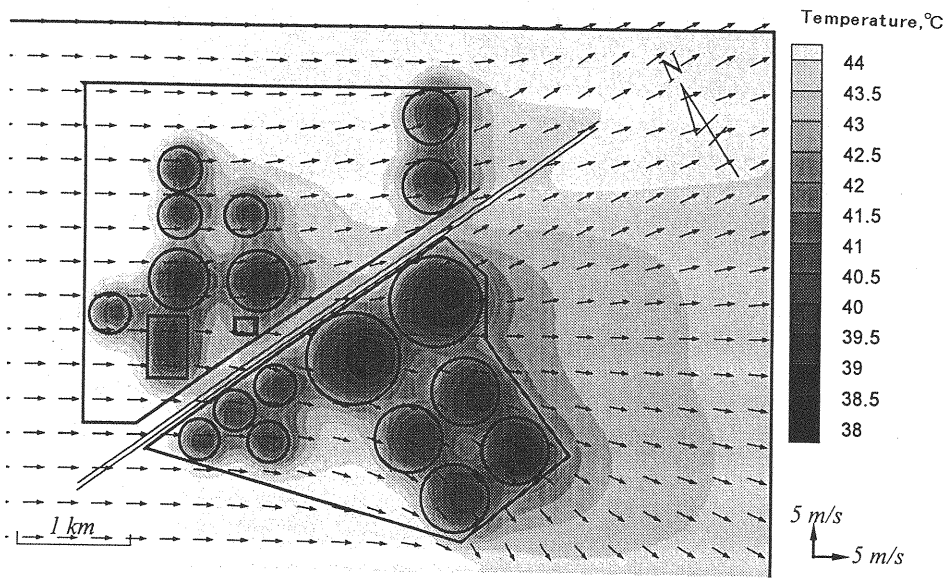

Fig. 16 Computed Horizontal Air Temperature and Wind distributions at 15:00 for Sept. 3.

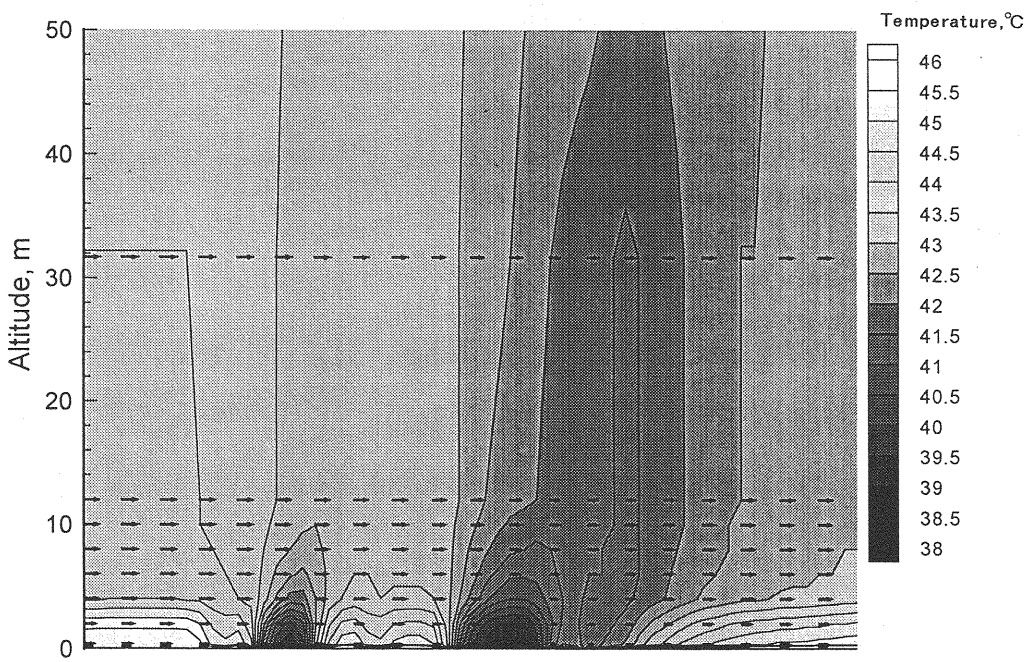

Fig. 17 Computed Vertical Air Temperature and Wind distributions at 15:00 for Sept. 3.

However, above *10 m* from the ground, such effects were almost indiscernible.

The ground temperature and the heat balance at the desert and at the alfalfa field sites were analyzed. It was found that the latent heat flux at the alfalfa filed exceeded the net radiation, and the rate of evapotranspiration was more than *10mm/day*, which is supported by data at similar farms elsewhere.

The numerical reproductions of the observed mitigation at the Sulaibiya Farm by the turbulence closure model was successful, and it showed the details of thermal structure.

These findings, as well as the data collected, will be fully utilized in the future plan of improving the thermal environment in arid area.

ACKNOWLEDGMENTS

The authors sincerely thank Mr. M. Maegaito, Dr. A. Iwabuchi, and Mr. Mark N. Sueyoshi of Desert & Environment Department, Shimizu Corporation, and Aridland Agriculture & Biotechnology Departments in KISR(Kuwait Institute for Scientific Research) for their significant contributions to field observations. The present study is supported by the KISR/PEC (Petroleum energy center) joint research program, "Analyses of Micro-climate Modification by the Kuwait Greenery Project".

REFERENCES

1. A. Wake : Analyses of Micro-climate Modification by the Kuwait Greenery Project, Green Age (by Petroleum Energy Center), December 1995, Vol. 7, pp. 10-14, 1995.
2. A. J. Dyer and B. B. Hicks : Flux-gradient relationships in the constant flux layer, Quarterly Journal of the Royal Meteorological Society, Vol. 96, pp. 715-721, 1970.
3. C. H. M. Van Bavel : Potential Evaporation : The Combination Concept and Its Experimental Verification, Water Resources Res., Vol. 2, pp. 455-467, 1966.
4. G. L. Mellor and T. Yamada : A hierarchy of Turbulent Closure Models for Planetary Boundary Layers, Journal of Atmospheric Sciences, Vol. 31, pp. 1791-1806, 1974.
5. H. A. Panofsky : Determination of Stress from Wind and Temperature Measurements, Quarterly Journal of the Royal Meteorological Society, Vol. 23, pp. 495-502, 1963.
6. J. Kondo, N. Saigusa and T. Sato : A Parameterization of evaporation from bare soil surface, Journal of Applied Meteorology, Vol. 29, pp. 385-389. 1990.
7. J. Louis : A Parametric Model of Vertical Eddy Fluxes in the Atmosphere, Boundary Layer Meteorology, Vol. 17, pp. 187-202, 1979.
8. J. R. Garratt and B. B. Hicks : Momentum, Heat, and Water Vapor Transfer to and from Natural Artificial Surfaces, Quarterly Journal of the Royal Meteorological Society, Vol. 99, pp. 680-687, 1973.
9. Norman J. Rosenberg and Shashi B. Verma : Extreme Evapotranspiration by Irrigated Alfalfa : A Consequence of the 1976 Midwestern Drought, Journal of Applied Meteorology, Vol. 17, pp. 934-941, 1978.
10. Peter S. Eagleson : Dynamic Hydrology, McGraw-Hill, 1970.
11. T. Yamada : Simulations of Nocturnal Drainage Flows by a q^2l Turbulence Closure Model, Journal of Atmospheric Sciences, Vol. 40, pp. 91-106, 1983.

APPENDIX - NOTATION

The following symbols are used in this paper:

a = surface albedo;
B_1 = empirical constants(=16.6);
e^2 = twice the turbulence kinetic energy;
f = Corioli's parameter;

G = surface level;
g = acceleration of gravity;
$\overline{H}$ = material surface of the model in z^*-coordinate;
H_f = sensible heat flux;
L_eE = latent heat flux;
l = turbulence length scale;
K = heat conductivity of soil;
K_x, K_{xy}, K_{yy} = horizontal eddy viscosity;
P_r = turbulent Prandtl number under neutral stability;
Q_v = mixing ratio of water vapor;
Q_{vGsat} = saturated specific humidity at the soil surface temperature;
q_v = deviation components of Q_v;
q_* = friction water vapor scale;
R_N = net radiation;
R_{Ln} = net long-wave radiation;
S = solar radiation;
S_M = stability function;
S_Q = empirical constants;
T = soil temperature;
t = time;
t_* = friction temperature;
U, V, W = wind components for x, y, z direction;
U_g, V_g = geostrophic wind components of U, V;
u, v, w, = deviation components of U, V, W;
u_* = friction velocity scale;
$-uw$, $-vw$, = turbulence momentum flux;
$-w\theta_v$ = turbulence heat flux;
$-wq_v$ = turbulence moisture flux;
W^* = vertical component of wind in the transformed coordinate;
x, y, z = Cartesian coordinate
z^* = transformed vertical coordinate;
z_g = ground elevation;
z_1 = reference height;
z_0, z_{0t} = roughness length for momentum and heat and/or moisture;
α = inverse of the turbulent plandtl number;
β = thermal expansion coefficient;
β_e = coefficients representing the surface moisture availability;
κ = von Karman constant;
ρ = air density;
ρC_p = heat capacity of air;
$\rho_s C_s$ = heat capacity of soil;
Θ_v = virtual potential temperature;
θ_v = deviation components of Θ_v; and
Ψ_m, Ψ_h = integrated stability correction terms for momentum and heat and/or moisture.

(Received December 11, 1996; revised February 2, 1998)